APS/123-QED

Complete time-reversed refocusing in reflection with an acoustic lagrangian model

Daniel G. Alfaro Vigo
Instituto de Matemática Pura e Aplicada, Est. D Castorina 110, Jardim Botânico, Rio de Janeiro, RJ 22460-320, Brazil.

André Nachbin
Instituto de Matemática Pura e Aplicada, Est. D Castorina 110, Jardim Botânico, Rio de Janeiro, RJ 22460-320, Brazil (author for correspondence).

Adolfo Guilherme Silva Correia
Instituto Militar de Engenharia, Praça Gen. Tibúrcio 80, CEP 22290-270, Rio de Janeiro–RJ, Brazil
(Dated: September 28, 2004)

This work presents discrete reflection-transmission acoustic models through which numerical experiments are performed efficiently. Each model is expressed through its corresponding reflection-transmission matrix and their connections with the continuous acoustic model are discussed in detail. Important physical phenomena are studied computationally. In particular reflection-transmission properties of waves in a rapidly varying random medim, which are valid over long propagation distances. By using a long computational domain, in a regime where we have Anderson localization, the energy of an incoherently scattered signal is entirely reflected back and, by time-reversal, completely recompressed into the smooth initial data. Another new result is the time-reversed refocusing, in reflection, of a wave train in the form of a bit stream. The robustness of the time-reversed refocusing phenomenon is outstanding.

PACS numbers: 43.20.Fn, 43.60.Tj, 02.60.Cb, 02.70.Bf

I. INTRODUCTION

Time-reversal techniques have emerged as a new important and fascinating discipline within wave propagation in heterogenous media [1, 2]. They are based on the use of a time reversal mirror, which is a device capable of receiving a signal in time, keeping it in memory and re-emitting it back into the medium in the reversed direction of time. The main effect is the refocusing of the scattered signal after time-reversal in a random medium: an acoustic pulse is sent in a disordered medium generating a "noisy" scattered signal which is time-reversed and sent back into the medium. The new scattered signal is a pure pulse with a shape similar to the initial pulse. Amazingly its "refocusing" takes place in time and space and seems to be independent of the realization of the medium. The pulse shape is of a deterministic character. This is called the stabilization of the refocused pulse shape and is due to the self-averaging property. Furthermore, in some situations the randomness of the medium helps to improve refocusing "beating" the difraction limit [3, 4]. Potential applications of these effects are numerous in imaging, wireless communication, medicine, geophysics, underwater acoustic, etc [5, 6, 16].

Several regimes and scalings can be adopted for studying this fascinating phenomenon. We chose to work in the regime where the medium's correlation length is smaller than the typical wavelength of the pulse, as quantified more precisely below. This choice has been made due to a great amount of well founded mathematical theory (in the corresponding wave/medium regime) that can be found, for example, in [7–9] and the references within. Nevertheless it is well known that this is not the only regime for time-reversed refocusing to take place. Results in the high-frequency regime (where the correlation length is comparable to the carrier wavelength) can be found in [3, 10–13].

From the theoretical point of view, a first proof of this refocusing effect has been obtained by Clouet and Fouque [14] in the context of a one-dimensional random medium for which only the time refocusing is relevant. The refocusing is obtained by using asymptotics in the regime where there are three well separated scales:

$$\frac{\text{correlation length}}{\text{pulse width}} \approx \frac{\text{pulse width}}{\text{propagation distance}} \ll 1.$$

That is the pulse propagates a long distance in comparison to its characteristic length through a medium that fluctuates on a fine scale relative to the pulse width. The fluctuations of the medium are not assumed to be small.

The aim of this paper is to present discrete reflection-transmission acoustic models through which we can perform numerical experiments in computational physics. In particular provide physical evidence of important properties related to the refocusing phenomenon in time-reversal. Of the simulations performed we highlight the complete refocusing of an incoherently reflected signal. By using a long computational domain, in a regime where we have *Anderson localization* [15], the entire energy of the initial data is back scattered as an incoherent signal. Time reversing this long incoherent signal gives rise to a smooth pulse identical to the initial profile. The incoherent signal is completely recompressed into a smooth pulse, hence illustrating the mathematical result given by Clouet and Fouque [14]. Another new result is the time-reversed refocusing, in reflection, of a wave train in the form of a bit stream. In a wireless communication application Kim, Blomgren and Papanicolaou [16] have studied the time-reversal of a wave train, in transmission. The robustness of the time-reversed refocusing phenomenon is outstanding. Robustness had already been analyzed in a different context, where the random medium changes slightly in between the forward and the time-reversed experiment. The corresponding stochastic theory and numerical results are presented in Alfaro *et al.* [17]. The numerical experiments were performed with the numerical scheme described (in detail, for the first time) in the present paper. The agreement between the theoretical expressions and numerical results were excellent. We recall that in the present paper we consider the time-reversal and refocusing of acoustic waves. Nevertheless the partial differential equations used are very similar to (linear) gravity driven (surface) water waves, propagating in shallow one-dimensional channels in the regime where the fluid is considered to be inviscid and incompressible. The randomness comes from the topography at the bottom of the shallow channel. All results presented also apply to this other physical application.

We focus our experiments on the time-reversal in reflection (TRR) regime, which has been much less explored than time-reversal in transmission (TRT) [1, 3, 6, 10–13]. Also because for TRR the recompression of highly incoherent (reflected) signals is seen in a more dramatic fashion. The authors' previous work in this regime can be found in [17–19] For example with our efficient discrete model we present an experiment in which we are able to clearly capture the phenomenon of *Anderson localization* [15]. For TRR it is the incoherent backscattered signal that is time-reversed. The transmitted wave (ballistic or not) is never used. Therefore we give an example where there is (effectively) no transmission whatsoever. This is a manifestation of Anderson localization. The random medium is opaque to all frequencies. As will be described in detail, we use a semi-lagrangian approach, readily controlling the left- and right-going wave fields and consequently the radiation boundary conditions at the extreme of the numerical domain. This enables the use of extremely long computational domains together with very long recording times, in a very efficient manner. This is essential for capturing phenomena such as Anderson localization.

Recently Sølna [20] presented interesting numerical results for TRR, in the high frequency regime, for an impulsive source interacting with weak fluctuations in a Goupillaud medium. In contrast, we time-reverse the incoherent backscattered signal generated by a broad pulse interacting with a strongly fluctuating medium. Our medium is not composed of slabs of equal traveltime (as in a Goupillaud medium; c.f. appendix A). Another interesting numerical work is given by [21] in which again the Goupillaud structure is taken advantage of numerically by using the Green's function over each subinterval. The evolution is done in frequency space (through a frequency dependent transfer matrix) and a boundary integral formulation leads to an efficient banded system to be solved numerically. In constrast our discrete lagrangian model leads to transfer (reflection-transmission) matrices in physical space. These 2 by 2 matrices (corresponding to the two characteristics of the underlying hyperbolic system) are easily inverted and the system is solved analytically. At no stage our implicit discrete scheme requires the solution of an algebraic system of equations. Moreover the discrete scheme can be applied to acoustic media more general than the Goupillaud medium.

This paper is organized as follows, in Section II we present the model of a continuous one-dimensional acoustic medium, and for completeness in the Section A the discrete case, i.e. a Goupillaud layered medium. In Section III we briefly present the asymptotic theory of time-reversal refocusing. In Section IV the numerical discretization of the equations is carried out, remarking the relationship with the layered medium case (appendix A) and setting up a numerical framework for experiments. Finally, in Section V we present some numerical experiments illustrating time-reversal refocusing and the advantages of our numerical framework.

II. ONE-DIMENSIONAL ACOUSTIC WAVES

The governing equations for wave propagation through a one-dimensional acoustic medium are the conservation laws for momentum and mass:

$$\varrho \partial_t u + \partial_z p = 0 \tag{1a}$$

$$\frac{1}{\kappa}\partial_t p + \partial_z u = 0, \tag{1b}$$

where $p(z,t)$ is the pressure and $u(z,t)$ the velocity. The medium coefficients $\varrho(z)$ and $\kappa(z)$ are, respectively, the density and bulk modulus, and the acoustic sound speed is given by

$$c(z) = \sqrt{\frac{\kappa(z)}{\varrho(z)}}. \tag{2}$$

The characteristics curves are defined as solutions of the ordinary differential equations $\frac{\mathrm{d}z}{\mathrm{d}t} = \pm c(z)$, which are highly oscillatory when the medium properties vary rapidly in space. Some authors [21] prefer to formulate problem (1) as a second order partial differential equation for the pressure:

$$\partial_{tt} p - c^2(z)\ \left(\rho\ \partial_z(\frac{1}{\rho}\partial_z p)\right) = 0,$$

which in the case where $\varrho =$ constant becomes the classical wave equation with variable wave speed. By introducing (as a new 'space-related' coordinate) the travel time from the origin

$$x = \int_0^z \frac{\mathrm{d}s}{c(s)}, \tag{3}$$

system (1) can be put in the form

$$\zeta \partial_t u + \partial_x p = 0 \tag{4a}$$
$$\partial_t p + \zeta \partial_x u = 0 \tag{4b}$$

where ζ is the acoustic impedance of the medium defined as

$$\zeta(x) = \sqrt{\varrho(x)\kappa(x)}. \tag{5}$$

We remark that due to the change of variable (3) system (4) has a family of characteristic lines

$$C_\alpha^\pm : \{x = x^\pm(t) = \pm t + \alpha\}, \quad \alpha \in \mathbb{R}, \tag{6}$$

as opposed to the highly oscillatory characteristics of system (1). Moreover in the homogeneous case, with ζ constant, it has the Riemann invariants

$$D = \zeta^{\frac{1}{2}} u + \zeta^{-\frac{1}{2}} p \tag{7a}$$
$$U = -\zeta^{\frac{1}{2}} u + \zeta^{-\frac{1}{2}} p \tag{7b}$$

representing right- and left-going waves respectively. By applying the operators $\partial_t \pm \partial_x$ to (7) and using (4) we obtain

$$(\partial_t + \partial_x) D = -rU \tag{8a}$$
$$(\partial_t - \partial_x) U = rD \tag{8b}$$

with the reflectivity coefficient

$$r(x) = \frac{\zeta'}{2\zeta} = \frac{1}{2}(\log \zeta)' = \frac{(\zeta^{1/2})'}{\zeta^{1/2}}. \tag{9}$$

We clearly see that in a homogeneous medium D is a traveling wave to the right and U to the left, and that they are completely uncoupled. The coupling of the Riemann invariants is through the reflectivity, in the forcing term. The multiple scattering nature of this model is evident through the constant exchange of energy between the left and right propagating modes.

Conservation of mechanical energy is another important feature concerning acoustic wave propagation. For solutions of (4) it takes the form

$$E(t) = \frac{1}{2}\int_{-\infty}^{+\infty} (\rho u^2 + \frac{1}{\kappa} p^2) \mathrm{d}z = \text{constant} \tag{10}$$

and according to the transformations introduced above, in the new variables, the following identity holds:

$$E(t) = \frac{1}{4}\int_{-\infty}^{+\infty} (D^2 + U^2) \mathrm{d}x = \text{constant}. \tag{11}$$

In the next section we will discuss a situation where the leading front of the transmitted wave seems to be under a diffusive like behavior. This is an apparent diffusion since the energy being lost (in a diffusive like manner) by say mode D is being stored as incoherent energy in mode U. The total energy is being conserved as expressed through the conservation law (11).

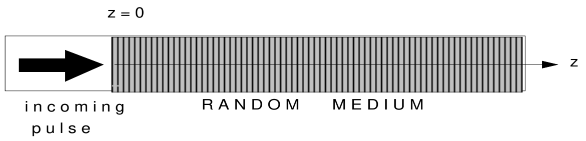

FIG. 1: A schematic representation of the random medium.

III. TIME-REVERSED REFOCUSING IN REFLECTION

In this section we outline the theory for time-reversed refocusing in reflection. For additional details we refer the reader to [14, 22]. We discuss the regime of separation of scales in which the ratio of the correlation length of the medium fluctuations to typical pulse wavelength are small and, comparable to the ratio of the typical wavelength to propagation distance. The medium considered is a random half-space with its corresponding properties modeled through the variable coefficients as

$$\varrho(z) = \begin{cases} \varrho_0\left(1 + \eta(\frac{z}{\varepsilon})\right), & \text{for } z \geq 0 \\ \varrho_0, & \text{for } z < 0 \end{cases} \tag{12a}$$

$$\frac{1}{\kappa(z)} = \begin{cases} \frac{1}{\kappa_0}\left(1 + \nu(\frac{z}{\varepsilon})\right), & \text{for } z \geq 0 \\ \frac{1}{\kappa_0}, & \text{for } z < 0. \end{cases} \tag{12b}$$

Here the background properties, expressed through ϱ_0 and κ_0, are constant. A schematic picture is presented in Fig. 1. The theory [14, 22] allows for background variations but for simplicity we present our overview in this simpler scenario. In one set of numerical experiments we will consider background variations. The random fluctuations are determined through the centered stationary stochastic processes $\eta(\cdot)$, $\nu(\cdot)$, which are bounded by a deterministic constant (i.e. $|\eta| < C$, $|\nu| < C$, with $C < 1$). They are considered exponentially mixing in the sense that (each) decorrelates exponentially fast, and have a correlation length of $O(1)$. The above scaling assures that the random fluctuations have correlation length of $O(\varepsilon)$, and we assume that $\varepsilon > 0$ is a small parameter. Under this scaling the heterogeneous medium is rapidly varying with respect to the propagating pulse of $O(1)$ width. We remark that we do not consider the fluctuations to be small.

In the homogeneous half-space $z < 0$ the Riemann invariants D, U correspond to right- and left-going waves. Thus the original wave fields are easily obtained through

$$u(z,t) = \frac{D_0(t - z/c_0) - U_0(t + z/c_0)}{2\zeta_0^{1/2}}$$

$$p(z,t) = \frac{\zeta_0^{1/2}}{2}\left(D_0(t - z/c_0) + U_0(t + z/c_0)\right),$$

where $c_0 = \sqrt{\kappa_0/\varrho_0}$, $\zeta_0 = \sqrt{\varrho_0 \kappa_0}$ are the sound speed and acoustic impedance in the homogeneous half-space.

We have used the notation $D_0(t) = D(x=0,t)$, $U_0(t) = U(x=0,t)$. For a pulse impinging upon the heterogeneous half-space from the left we have, at the interface, the reflected signals

$$u^{\mathrm{ref}}(0,t) = -\frac{U_0(t)}{2\zeta_0^{1/2}}, \qquad p^{ref}(0,t) = \frac{\zeta_0^{1/2} U_0(t)}{2}.$$

If we consider a pulse with typical wavelength of $O(1)$ and observe its evolution for a relatively small time, since the correlation length of the fluctuations (12) is of $O(\varepsilon)$, one sees according to homogenization theory that the pulse practically does not generate reflection and travels with velocity c_0 without changing its shape [23]. However, if we continue observing for a longer time, reflections appear and the pulse moves with a random speed and changes its shape, in a deterministic fashion, according to the O'Doherty-Anstey (ODA) approximation (see [22, 23]). To leading order the deterministic pulse shaping is diffusive-like. In accordance with these remarks, the time reversal procedure should be implemented for a sufficiently large time intervals.

The time reversal procedure goes as follows: (i) let a right-going pulse impinge upon the heterogeneous half-space, (ii) record the reflected time signal at the interface up to a time t_0 and (iii) reverse its time direction. Hence this incoherent signal is used as new initial data being re-emitted back into the medium. A new reflected signal is generated at the interface and its subsequent refocusing can be stated as follows: if we observe this time-reversed reflection for a sufficiently long time ($t > t_0$) then a left-going pulse, that resembles the initial one, emerges at the interface exactly at $t = t_0$ and continues to travel to the left, into the homogeneous medium. This will be shown in the numerical experiments.

Mathematically this property is established through an asymptotic analysis (as $\varepsilon \downarrow 0$) for the stochastic differential equations which model the pulse reflection process (for details see [14, 22]). In this analysis the scaling is crucial for establishing the diffusion approximation that allows for the use of the powerful tools of stochastic calculus.

More precisely, we consider that the recording and observation times are long and satisfy $t_0 = \varepsilon^{-1}t_0'$ and $t_1 = \varepsilon^{-1}t_1'$, respectively. We could allow for amplification and distortion of the recorded signal (at the time reversal mirror) by the form through which we introduce the cutoff function $G_{t_0}(t)$, supported on the interval $[0, t_0]$. This function represents (mathematically) the recording process and is considered to vary slowly, in the sense that

$$G_{t_0}(t) = G_{t_0'}(\varepsilon t)$$

where $G_{t_0'}$ is smooth in $(0, t_0')$. In the simplest situation, when one does not include amplification or distortion effects, $G_{t_0} = \mathbf{1}_{[0,t_0]}$ the indicator function for the interval $[0, t_0]$.

We now recall the main results from the asymptotic stochastic theory for time-reversal in reflection. These results are needed in order to understand the nontrivial results produced by the discrete model. The refocusing property is stated as follows. For an initial right-going pulse $D_0(t) = f(t)$ (as $\varepsilon \downarrow 0$) the limiting time-reversed reflection observed at the time t_1 satisfies [14]:

$$\lim_{\varepsilon\downarrow 0} U_0^{\varepsilon,\mathrm{TR}}\left(\frac{t_1'}{\varepsilon} + t\right) = \begin{cases} f^{\mathrm{TR}}_{G_{t_0'}}(t), & \text{for } t_1' = t_0' \\ 0, & \text{for } t_1' \neq t_0' \end{cases} \tag{13}$$

where the refocused time reversed (TR) pulse is

$$f^{\mathrm{TR}}_{G_{t_0'}}(t) = \big(H_{G_{t_0'}}(\cdot) \star f(-\cdot)\big)(t) \tag{14}$$

with the (limiting) refocusing kernel $H_{G_{t_0'}}(\cdot)$ given by

$$\hat{H}_{G_{t_0'}}(\omega) = \big(\Lambda(\omega,\cdot) \star G_{t_0'}(-\cdot)\big)(0). \tag{15}$$

By $\hat{g}$ we represent the Fourier transform of the function g and the symbol $\star$ stands for convolution with respect to t. The stochastic theory gives rise to the *power spectral density* $\Lambda(\omega,t)$ which is a deterministic function given by (see [7, 22])

$$\Lambda(\omega,t) = \frac{\omega^2\gamma_n}{(1+\omega^2\gamma_n t)^2} \tag{16}$$

with

$$\gamma_n = \frac{1}{c_0}\int_0^\infty \mathbb{E}\{n(s)n(s+r)\}\mathrm{d}r, \tag{17}$$

and $n(s) = (\eta(s) - \nu(s))/2$ (c.f. (12)).

A remarkable point is that the limiting form for the (time-reversed) refocused pulse (i.e. when $t_1' = t_0'$) is deterministic and depends only on one statistical property of the random medium as indicated in (14)–(17). This result is known as *pulse stabilization* (see [14, 22, 23]). Actually, in deriving equation (13) one uses convergence in probability, which means that the observed refocused pulse stays arbitrarily close to the deterministic signal (14) with a probability that approaches one as $\varepsilon \downarrow 0$. This will be illustrated through our numerical scheme.

As mentioned above, a better understanding on the shape of the refocused pulse is achieved by analysing the case of a time reversal mirror without distortions, namely with $G_{t_0'} = \mathbf{1}_{[0,t_0']}$. We simplify notation by using the subscript t_0' in place of $G_{t_0'}$ in the representation of the corresponding refocused pulse and refocusing kernel. In this particular case we get that the Fourier transform of the refocusing kernel $H_{t_0'}$ is given by

$$\hat{H}_{t_0'}(\omega) = \frac{\omega^2\gamma_n t_0'}{1+\omega^2\gamma_n t_0'}. \tag{18}$$

Furthermore, we see that

$$\hat{H}_{t_0'}(\omega) \approx \omega^2\gamma_n t_0' \quad \text{for } |\omega| \text{ small}$$

and

$$\hat{H}_{t_0'}(\omega) \approx 1 - \frac{1}{\omega^2 \gamma_n t_0'} \quad \text{for } |\omega| \text{ large.}$$

Therefore $H_{t_0'}$ is a highpass filter. Moreover, when t_0' goes to infinity $H_{t_0'}$ tends to a Dirac δ-function. This observation is apparent from the estimate

$$\|f_{t_0'}^{\mathrm{TR}}(\cdot) - f(-\cdot)\|_\infty \leq \frac{c_1 \|\hat{f}\|_\infty}{\sqrt{\gamma_n t_0}}$$

where $\|g\|_\infty = \sup_{t\in\mathbb{R}} |g(t)|$ represents the usual L^∞-norm of $g(t)$ and c_1 is a positive real constant. So we have that as the recording time grows, the limiting refocused pulse shape uniformly approaches the initial pulse waveform. Hence the original pulse is fully recovered through time reversal in reflection. The long incoherent reflected signal recompresses into the smooth initial profile. This has never been shown numerically and is reminiscent of Anderson localization [15]. Namely the random medium is opaque (to all wavenumbers) and there is no transmission. All the energy is reflected back and by time reversed recompression the initial pulse is fully recovered. Moreover, for the limiting time-reversed reflection, after some elementary estimates we get that if $\|G_{t_0'}(t')\|_\infty \leq 1$ then

$$\|f_{G_{t_0'}}^{\mathrm{TR}}\|_2 \leq \|f_{t_0'}^{\mathrm{TR}}\|_2, \tag{19}$$

where $\|g\|_2 = (\int |g(t)|^2 \mathrm{d}t)^{1/2}$ represents the L^2-norm of the time-signal $g(t)$. Furthermore, this is a sharp estimate and if additionally we only consider non-negative cutoff functions then the equality holds if and only if $G_{t_0'} = \mathbf{1}_{t_0'}$. Hence the uniform cutoff function is the best for energy recovery through recompression.

IV. DISCRETE REFLECTION-TRANSMISSION SYSTEMS

In this section we analyse discrete reflection-transmission systems which can be used, for example, in numerical experiments. We present two ways of obtaining the discrete physical models. First by numerical methods for approximating the system of partial differential equations. We show that in one particular case we obtain a Goupillaud medium commonly used in Geophysics. Both finite difference schemes presented have a discrete analog for the energy conservation law. We also study a discrete physical model by approximating evolution operators.

We shall develop numerical schemes for the solution of the system (1), basing our analysis on the equivalent equations (8) that are more suitable for the study of the right- and left-going waves, and therefore for reflection-transmission problems. As mentioned earlier, the velocity and pressure fields can be easily obtained by using transformation (7). The change of variable (3) can be carried out accurately by solving the corresponding initial value problem (in z) through a suitable method. For simplicity, in describing the numerical schemes, we consider that this coordinate change has been performed exactly.

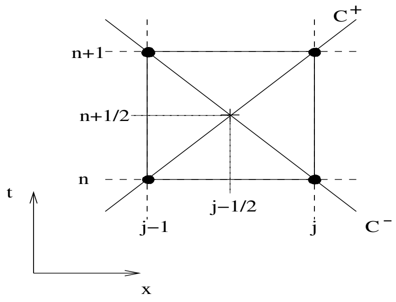

FIG. 2: Characteristic lines, spatio-temporal grid and staggered gridpoints.

We call our numerical models as *discrete physical models* because they are all defined in physical space, rather than in frequency space as many authors do. Moreover the random medium does not need to be piecewise constant. Thus we explicitly obtain reflection-transmission matrices corresponding to the discrete scattering process for quite general random media profiles. We point out that all schemes presented are unconditionally stable. Moreover the implicit schemes developed are such that there is no need to solve an algebraic system of equations.

A. Semi-lagrangian schemes

The semi-lagrangian approach in the computation of highly oscillatory solutions to hyperbolic differential equations has been successfully used. An important reason for this, is its ability to perform the correct advection of high frequency modes, eliminating one of the central source of problems in the discrete approximations of the equations [24, 25]. We shall follow this approach in the discretization of (8) to obtain an unconditionally stable scheme.

We consider the spatio-temporal grid $\{(x_j, t_n),\ j \in \mathbb{Z}, n \in \mathbb{Z}_+\}$ with $\Delta x = \Delta t = h$ and use the representation

$$\begin{aligned} D_j^n &= D(x_j, t_n) \\ U_j^n &= U(x_j, t_n) \end{aligned}$$

where $(x_j, t_n) = (jh, nh)$.

We shall approximate equation (8) in the staggered gridpoints $(x_{j-1/2}, t_{n+1/2})$ (see Fig. 2). The differential operators $\partial_t \pm \partial_x$ are discretized by considering them as directional derivatives along the characteristics $C^\pm$ using a central difference approximation. The right hand side D, U are approximated by a midpoint averaging on the characteristics $C^{\pm}$, respectively, and the reflectivity coefficient (9) using a finite difference approximation supported on the spatial grid points. We obtain

$$\frac{D_j^{n+1} - D_{j-1}^n}{h} = -\tilde{r}_{j-1/2}\Big(\frac{U_{j-1}^{n+1} + U_j^n}{2}\Big) \quad (20a)$$

$$\frac{U_{j-1}^{n+1} - U_j^n}{h} = \tilde{r}_{j-1/2}\Big(\frac{D_j^{n+1} + D_{j-1}^n}{2}\Big) \quad (20b)$$

where $\tilde{r}_{j-1/2}$ represents the approximation of the reflectivity coefficient. There are different ways to approximate the reflectivity, which gives place to different discrete reflection-transmission models. In particular we will show that one of our choices falls exactly on the Goupillaud medium commonly used by geophysicists in seismic analysis.

For instance, we can use one of the following approximations:

$$\tilde{r}_{j-1/2} = \frac{\log\zeta_j - \log\zeta_{j-1}}{2h} = \frac{1}{2h}\log\Big(\frac{\zeta_j}{\zeta_{j-1}}\Big) \quad (21a)$$

or

$$\tilde{r}_{j-1/2} = \frac{\left(\frac{\zeta_j^{1/2} - \zeta_{j-1}^{1/2}}{h}\right)}{\left(\frac{\zeta_j^{1/2} + \zeta_{j-1}^{1/2}}{2}\right)} = \frac{2}{h}\Big(\frac{\zeta_j^{1/2} - \zeta_{j-1}^{1/2}}{\zeta_j^{1/2} + \zeta_{j-1}^{1/2}}\Big) \quad (21b)$$

which formally lead to second-order numerical schemes.

Regarding the implicit relation between D and U we solve a 2×2 system to get that

$$\begin{pmatrix} D_j^{n+1} \\ U_{j-1}^{n+1} \end{pmatrix} = \begin{bmatrix} \tilde{\tau}_{j-1/2} & -\tilde{\sigma}_{j-1/2} \\ \tilde{\sigma}_{j-1/2} & \tilde{\tau}_{j-1/2} \end{bmatrix} \begin{pmatrix} D_{j-1}^n \\ U_j^n \end{pmatrix} \quad (22)$$

where

$$\tilde{\tau}_{j-1/2} = \frac{1 - (h^2/4)\tilde{r}_{j-1/2}^2}{1 + (h^2/4)\tilde{r}_{j-1/2}^2},$$

$$\tilde{\sigma}_{j-1/2} = \frac{h^2\tilde{r}_{j-1/2}^2}{1 + (h^2/4)\tilde{r}_{j-1/2}^2},$$

are the *discrete* transmission and reflection coefficients, respectively. Therefore the matrix above defines the discrete reflection-transmission matrix at the staggered mesh point $x_{j-1/2}$.

Since these reflection-transmission matrices are orthogonal we obtain the following discrete analog for the energy conservation law

$$\sum_{j\in\mathbb{Z}}\Big((D_j^{n+1})^2 + (U_j^{n+1})^2\Big) = \sum_{j\in\mathbb{Z}}\Big((D_j^n)^2 + (U_j^n)^2\Big). \quad (23)$$

Therefore, the schemes presented are conservative and consequently unconditionally stable in the discrete L^2-norm. Thus taking into account that it is second-order accurate, convergence follows directly from stability and consistency of the scheme. However, since we deal with rapidly varying acoustic media and high frequency wave fields (cf. equation (12)) accuracy in fact depends on how well the high frequency modes are represented by the computational grid. This imposes restrictive conditions on the mesh size but only due to accuracy requirements and not due to stability.

We call attention to the analogy between the relations above and the equations for a Goupillaud medium (see the appendix A). Specifically, by using the approximation (21b), the reflection-transmission matrices of the scheme and a Goupillaud layered medium coincide. In this case the numerical scheme can be interpreted as approximating the acoustic medium by a Goupillaud medium. The Goupillaud medium is frequently used in Geophysics.

B. Operator splitting scheme

System (8) can be re-written in a more compact operator notation

$$\partial_t \mathbf{a} = \mathrm{H}(x, \partial_x)\mathbf{a}$$

where

$$\mathbf{a} = \begin{pmatrix} D \\ U \end{pmatrix} \quad \text{and} \quad \mathrm{H}(x,\partial_x) = \begin{bmatrix} -\partial_x & -r(x) \\ r(x) & \partial_x \end{bmatrix}.$$

The operator H can be decomposed as the sum of a constant-coefficient diagonal hyperbolic operator $\mathrm{H}_\mathbf{0}$ and a multiplicative operator M defined as

$$\mathrm{H}_\mathbf{0}(\partial_x) = \begin{bmatrix} -\partial_x & 0 \\ 0 & \partial_x \end{bmatrix} \quad \text{and} \quad \mathrm{M}(x) = \begin{bmatrix} 0 & -r(x) \\ r(x) & 0 \end{bmatrix},$$

with associated evolution equations

$$\partial_t \mathbf{a} = \mathrm{H}_\mathbf{0}\mathbf{a} \quad (24a)$$

and

$$\partial_t \mathbf{a} = \mathrm{M}\mathbf{a}, \quad (24b)$$

respectively. We assume that $r(x)$ is continuous and bounded. The evolution (solution) operators $\mathcal{H}_0$ and $\mathcal{M}$ associated to equations (24) are unitary. Their action on a vector valued function is readily available and we have

$$\mathcal{H}_0(t)\begin{pmatrix} D(x) \\ U(x) \end{pmatrix} = \begin{pmatrix} D(x-t) \\ U(x+t) \end{pmatrix},$$

$$\mathcal{M}(t)\begin{pmatrix} D(x) \\ U(x) \end{pmatrix} = \begin{bmatrix} \cos(r(x)t) & -\sin(r(x)t) \\ \sin(r(x)t) & \cos(r(x)t) \end{bmatrix}\begin{pmatrix} D(x) \\ U(x) \end{pmatrix}.$$

Introducing a temporal grid with time step Δt and using the Strang splitting scheme [26], we obtain the semi-discrete conservative scheme

$$\mathbf{a}^{n+1} = \mathcal{H}_0\Big(\frac{\Delta t}{2}\Big)\mathcal{M}(\Delta t)\mathcal{H}_0\Big(\frac{\Delta t}{2}\Big)\mathbf{a}^n \quad (25)$$

which is consequently unconditionally stable. Note that no approximation have been performed in space. For initial data and reflectivity coefficient sufficiently regular, it is second order accurate in time, thus convergence in the L^2-norm follows. Moreover, if $r(x)$ is only continuous and bounded the scheme is consistent [27] and consequently convergent.

For the numerical applications we introduce spatial mesh points $\{x_j = j\Delta x | j \in \mathbb{Z}\}$ and adopt approximate values $\tilde{r}(x)$ for the reflectivity coefficient. Therefore we obtain the approximate evolution operator $\tilde{\mathcal{M}}$. After replacing it in (25) we get the splitting scheme

$$\mathbf{a}^{n+1} = \mathcal{H}_0(\frac{\Delta t}{2})\tilde{\mathcal{M}}(\Delta t)\mathcal{H}_0(\frac{\Delta t}{2})\mathbf{a}^n. \tag{26}$$

At this stage the medium has been discretized but not the solution modes D and U. This discrete model is also conservative, but inherits truncation errors from the space discretization. For instance, using a central difference approximation for the reflectivity coefficient it becomes second order in space and time.

By using a time step $\Delta t = \Delta x$ we avoid the introduction of interpolation errors since the characteristic lines go through the mesh points. Going through a complete discretization also in D and U, and rearranging terms, the semi-discrete expression above takes the form

$$\begin{pmatrix} D_j^{n+1} \\ U_{j-1}^{n+1} \end{pmatrix} = \begin{bmatrix} \cos(\tilde{r}_{j-1/2}\Delta t) & -\sin(\tilde{r}_{j-1/2}\Delta t) \\ \sin(\tilde{r}_{j-1/2}\Delta t) & \cos(\tilde{r}_{j-1/2}\Delta t) \end{bmatrix} \begin{pmatrix} D_{j-1}^n \\ U_j^n \end{pmatrix}. \tag{27}$$

We again have a corresponding discrete reflection-transmission matrix for the scheme. Moreover, by approximating $\cos(\tilde{r}_{j-1/2}\Delta t)$ and $\sin(\tilde{r}_{j-1/2}\Delta t)$ by their second order Padé approximants, we obtain (22).

V. TIME-REVERSAL EXPERIMENTS

In this section we present numerical illustrations of the refocusing of time-reversed reflections. For $h \ll 1$, small enough, all discrete models give similar results. We present the results for model (20) with the first discrete reflectivity given by (21).

The numerical experiments are conducted as follows:

1. we let a pulse-shaped wave impinge upon the random medium.

2. we record the reflected wave at the left extreme as a time signal, and re-enter it into the medium after time-reversion, by considering it as a time-dependent boundary condition along the incoming characteristic (cf. Fig. 3). Along the homogeneous region the incoming and outgoing signals (D and U) are decoupled.

An equivalent procedure, frequently used, consists of capturing a spatial segment of the reflected signal travelling to the left in the homogeneous half-space, at a particular time instant; 'freezing' this piece and sending it back into the heterogeneous medium as a secondary right propagating source wave.

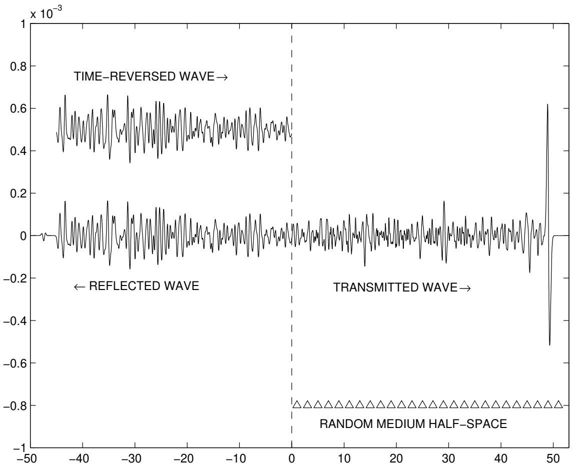

FIG. 3: The forward experiment for the time reversal procedure. The signal in the negative part of the domain is out of the computational domain and has been recorded in time as indicated in the (vertically) shifted signal. This signal is time reversed and sent back into the random medium as a time dependent boundary condition along the (left) incoming characteristic.

Since we shall compute the approximate solution for a finite time interval, from the hyperbolicity of the equations follows that only a slab of the heterogeneous half-space should be considered. Then the domain of interest is completed by adding little pieces of homogeneous medium to both sides of this slab, in order to correctly manage the radiation boundary conditions and also properly setting the initial incoming pulse/signal.

The heterogeneous (slab) medium properties are modeled by considering a constant compressibility κ_0 and setting random density values at points $\tilde{z}_j = j\varepsilon$ of the physical domain. This is done using a random number generator, so that $\rho(\tilde{z}_j) = \rho_0(1 + Y_j)$ where Y_j are independent random variables uniformly distributed over $(-C, C)$ with $0 < C < 1$. Connecting these values we define the medium as a piecewise linear function over the whole slab.

The computational mesh is constructed as follows: first the change of variables (3) is performed by maping analytically the points $\tilde{z}_j$, of the physical domain, into their travel time images $\tilde{x}_j$ in the computational domain. Then by a linear interpolation we obtain approximately the points z_k that maps to the uniform mesh defined by $x_k = kh$ and set the corresponding densities $\rho_k = \rho(z_k)$.

Concerning the mesh size h, a choice of 5-10 mesh points per layer gives excellent results. This is in agreement with the remarks on the numerical experiments presented in [8]. In [28] a spatial discretization with mesh size equal ε also produced very good results. The heuristic reasoning below can help us understand why the choice $h = c_1\varepsilon$, with a constant $c_1 < 1$, give us accurate results despite the fact that the conditions imposed by a classical consistency-accuracy analysis (see [29]) are not fulfilled.

Recall that according to the homogenization theory, for distances of the order of several typical wavelengths the pulse shape effectively does not change nor effective reflection is generated [23], thus a discretization that resolves the initial pulse is enough for a good representation of the effectively transmitted wave. In the other extreme for long propagation distances the pulse attenuates and spreads out as predicted by the O'Doherty-Anstey theory [23, 30], so again there is no need to increase resolution to capture the transmitted wave front. Additionally a lot of energy is transferred to the coda and also reflected back. More specifically, the power spectrum of the scattered wave at the interface has a maximum expected spectral power at the frequency $\omega = 1/\sqrt{\gamma_n t}$ [23, 31, 32] which is of $O(1)$. Therefore properly resolving the initial pulse warrants a good resolution of the scattered signal at the interface. Moreover, when $h = c_1\varepsilon$ the typical subwavelength scale reflected waves, mainly associated with high-order multiple scattering, are also well resolved.

We again remark that when the signal is recorded in space we need to use a mesh sufficiently large to accommodate for the entire reflected signal at the left side of the heterogeneous slab (as indicated in Fig. 3). Therefore the size of the computational domain increases proportionally to the propagation time t_0. However, the procedure implemented in our experiments uses a computational domain roughly of the size of the slab, independently of the length of the recording interval. This is due to the exact radiation condition defined through the (corresponding) outgoing characteristics.

A. Refocusing experiments

In all the experiments that follow we take $\varepsilon = 0.1$, and a mesh size $h = 0.01$. The heterogeneous slab has length L and the initial pulse is given by the Gaussian derivative

$$f(z) = -7(z-2)\exp\big(-\frac{(z-2)^2}{0.1}\big).$$

The cutoff function for the time-reversal mirror is the indicator of the time interval $[0, t_0]$.

1. *Complete refocusing and localization (Figures 4–6).*

In our first set we perform two experiments for a heterogeneous slab with $L = 405$. One is the forward experiment with the initial pulse generating (backscattered) reflections. This is followed by the time reversed experiment using the recorded reflected signal as initial data.

Fig. 4 shows the forward experiment with the ODA attenuation taking place along the wavefront. Time evolves from the bottom of the figure towards the top. At the bottom left (near zero) we have the initial (Gaussian derivative) pulse. As time evolves we see the diffusive like behavior along the leading pulse. Very little energy is being transmitted at the right end of the computational domain. At time $t = 500$ (the top trace) the small leading wavefront has propagated out of the computational domain without generating any spurious reflections. The reflected signal is recorded at the left end as it leaves the computational domain.

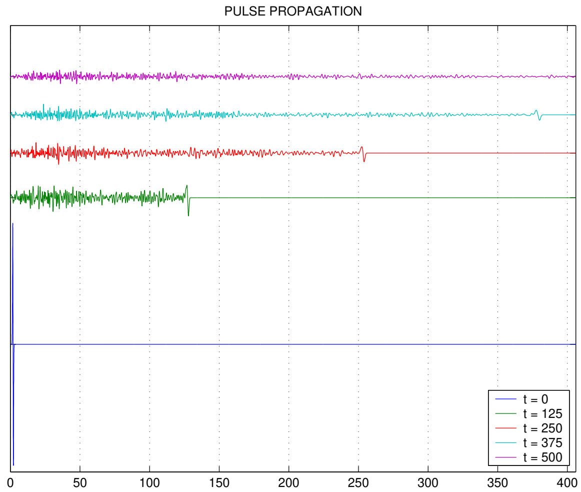

FIG. 4: Forward experiment. Propagating pulse at different times. Traces from bottom to top: $t = 0$, 125, 250, 375 and 500.

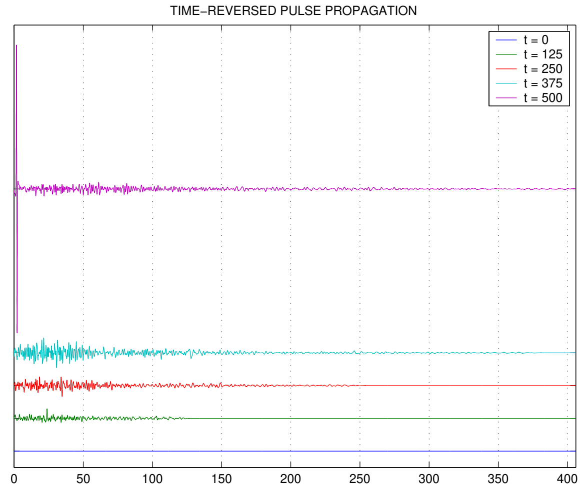

FIG. 5: Localization in the time-reversal experiment. Time-reversed incoherent signal for different times. Traces from bottom to top: $t = 0$, 125, 250, 375 and 500.

In Fig. 5 we have the time reversed experiment. At time $t = 0$ there is no activity in the random medium. The time reversed incoherent signal enters the computational domain as a time dependent boundary condition along the incoming characteristic, at the left end of the computational domain. The trace at time $t = 125$ (second from the bottom of Fig. 5) shows the incoherent signal entering from the left. This high frequency signal interacts very strongly with the random medium and all of its energy is (effectively) reflected back. This is a manifestation of *Anderson localization* and is clearly seen in the traces at times $t = 250$ and $t = 375$. There is basically no activity at the right end of the computational domain, which is effectively opaque. At the time predicted by the theory, we observe the recompression of the incoherent energy that is building up at the left end of the computational domain. Namely at time $t = 500$ incoherent energy recompresses into a smooth pulse.

In order to see better how good is the recompression we compare two time reversed experiments: one for which we recorded the reflected signal for $t_0 = 410$ and another which we recorded for a time interval twice as long ($t_0 = 820$). The result is shown in Fig. 6 where we compare the refocused pulses with the initial profile. It is clear that we have been able to recompress (effectively) 100% of the initial data's energy. As mentioned above, this is predicted by the theory and is a manifestation of localization: if the random medium is long enough we have zero transmission (the medium is opaque).

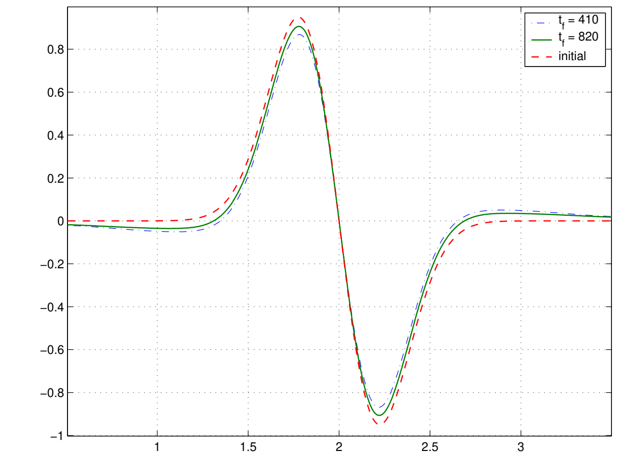

FIG. 6: Initial (dashed line) and refocused pulses for $t_0 = 410$ (dash-dotted line) and $t_0 = 820$ (solid line).

2. Refocused pulse stabilization (Figure 7).

In the next experiments we set $t_0 = 70$ and $L = 50$ and demonstrate the stabilization (self-averaging) of the refocused pulse by showing the results of 10 realizations of the heterogeneous slab. It is clear in Fig. 7 that the refocused pulse shape is deterministic, independing of the specific medium realization. Note also that the pulse's amplitude is smaller than in Fig. 6 because the recording time interval is smaller.

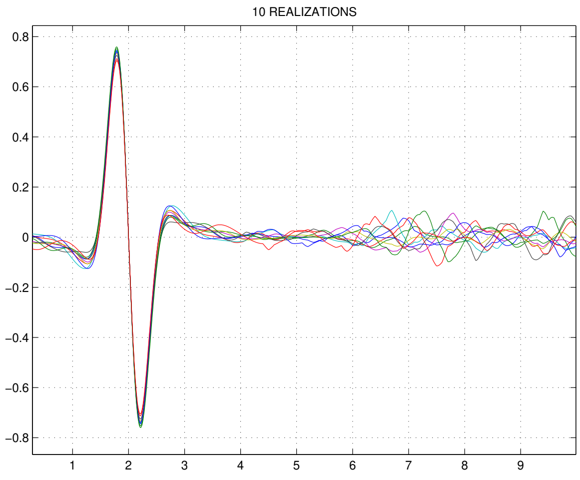

FIG. 7: Self-averaging of the refocused pulses over 10 realizations of the medium.

3. Background medium effect (Figure 8).

Now we experiment with a scenario that has not been explored before. In particular we will give evidence on the robustness of the refocusing phenomenon by gradually going against the separation of scales hypothesis, which is very important for developing the theory. In this example the background medium is not homogeneous: we define the *background* medium density by $\varrho_0(z) = 1 + 0.5\sin(2\pi m(z-5)/L)$ on a slab of length $L = 80$ and set $m = 4$, 32 and 64. The physical domain extends from $z_i = 0$ to $z_f = 84$ and the recording time $t_0 = 90$. In Fig. 8 we present the numerical results for a wide range of background scales. In particular for $m = 64$ the deterministic background scale is of the same order as the pulse. We note that as the medium varies on faster scale the refocused pulse has a larger amplitude. In any case the robustness of the incoherence recompression phenomenon (i.e. refocusing in reflection) is remarkable.

4. Wave train refocusing (Figure 9).

In this experiment we consider the refocusing of a pulse shaped wave train in the form of a bit stream, as presented at the top trace given in Fig. 9. This has never been done for time reversal in reflection. Each (initial) unit bit is described by the derivative of a Gaussian. The top trace in Fig. 9 is the initial bit stream **11011011011011011011011** where the support of a zero bit is the same as the effective support of the unit bit. The middle trace represents the incoherent reflection generated by the interaction of the bit stream with a disordered acoustic medium. Recall that the reflected trace is recorded at the left end of the acoustic channel, namely along the left going characteristic. The initial pulse shape (of each bit) and the bit stream order are

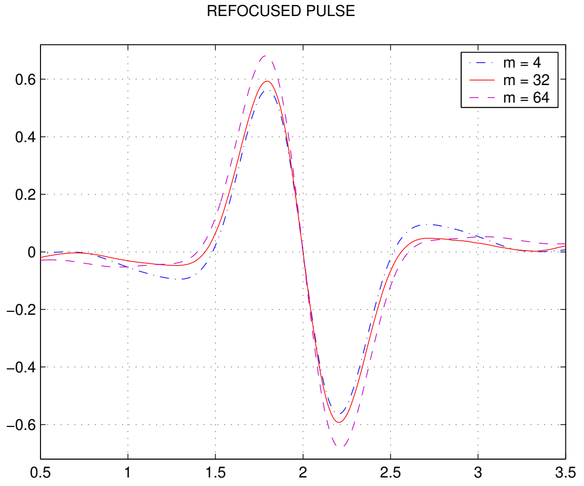

FIG. 8: Refocusing in the case of a background varying medium. We show the refocused pulses for $m = 4$ (dash-dotted line), $m = 32$ (solid line) and $m = 64$ (dashed line)

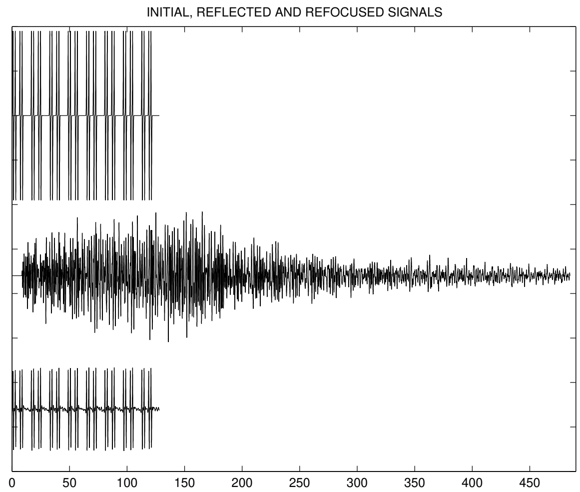

FIG. 9: Wave train refocusing. The horizontal axis is time for a signal recorded at the left end of the computational domain. The initial profile is presented at the top trace representing the bit stream **11011011011011011011011**. The incoherent reflected signal is presented at the middle trace and the (recompressed) refocused wave train at the bottom trace. The original bit stream is recovered.

now randomly suffled through the forward experiment. We have used a heterogeneous slab of length $L = 200$ within a physical domain from $z_i = 0$ to $z_f = 202$ and we set $t_0 = 485$. We then perform the time reversal procedure for the incoherent time-signal given at the middle trace of Fig. 9. Recall that we do not need to allocate the reflected and refocused signals on the computational mesh. This long, incoherent, time reversed signal is sent back into the random slab as a time dependent boundary condition at the left end of our computational domain. This boundary condition is imposed along the incoming characteristic, from the left. Again the robustness of the refocusing phenomenon is clearly seen at the bottom trace of Fig. 9. The recompression process is very efficient along the entire bit stream. In particular the zeros of the bit stream are recovered in a very "clean" fashion and we have a uniform amplitude distribution for the recompressed bits.

APPENDIX A: THE GOUPILLAUD LAYERED MEDIUM

Goupillaud layered media are frequently used as geophysical models [23, 30]. Due to the analogy mentioned in section IV, for the lagrangian schemes and the transmission-reflection relations for a layered medium, in this section we describe a Goupillaud layered medium. Here $\varrho(z)$ and $\kappa(z)$ are piecewise constant with jump discontinuities at interfaces, in such a way that the travel time across every layer is the same.

Therefore the interfaces are uniformly spaced at intervals of Δx in the travel time x coordinate and we use the notation

$$x_j = j\Delta x, \qquad f_j(\dots) = f(x_j, \dots), \quad j \in \tfrac{1}{2}\mathbb{Z},$$

for any function dependent on x.

Now, without loss of generality we consider the interfaces positioned at points $x_{j-1/2}$, $j \in \mathbb{Z}$ and by assuming the continuity of the pressure and velocity wavefields, from equations (7) we get the following jump conditions for the right- and left-side limits of $D(x,t)$ and $U(x,t)$, respectively, at the interface $x = x_{j-1/2}$

$$\begin{bmatrix} \zeta_{j-1}^{-1/2} & -\zeta_{j-1}^{-1/2} \\ \zeta_{j-1}^{1/2} & \zeta_{j-1}^{1/2} \end{bmatrix} \begin{pmatrix} D_{j-1/2-0}(t) \\ U_{j-1/2-0}(t) \end{pmatrix} = \begin{bmatrix} \zeta_{j}^{-1/2} & -\zeta_{j}^{-1/2} \\ \zeta_{j}^{1/2} & \zeta_{j}^{1/2} \end{bmatrix} \begin{pmatrix} D_{j-1/2+0}(t) \\ U_{j-1/2+0}(t) \end{pmatrix}. \tag{A1}$$

Moreover, since in each layer the underlying medium is homogeneous the Riemann invariants are conserved along the segments of characteristic lines between the interfaces, and by continuity

$$\begin{aligned} D_{j-1/2-0}(t + \Delta t/2) &= D_{j-1}(t) \\ D_{j-1/2+0}(t + \Delta t/2) &= D_j(t + \Delta t) \\ U_{j-1/2-0}(t + \Delta t/2) &= U_{j-1}(t + \Delta t) \\ U_{j-1/2+0}(t + \Delta t/2) &= U_j(t) \end{aligned}$$

where we have set $\Delta t = \Delta x$. Finally, by evaluating in (A1) for time $t + \Delta t/2$ and using the relations above we obtain the system

$$\begin{pmatrix} D_j(t+\Delta t) \\ U_{j-1}(t+\Delta t) \end{pmatrix} = \begin{bmatrix} \tau_{j-1/2} & -\sigma_{j-1/2} \\ \sigma_{j-1/2} & \tau_{j-1/2} \end{bmatrix} \begin{pmatrix} D_{j-1}(t) \\ U_j(t) \end{pmatrix} \tag{A2}$$

where the matrix standing in the right hand side is known as reflection-transmission matrix with the transmission and reflection coefficients defined, respectively, by

$$\tau_{j-1/2} = \frac{2\sqrt{\zeta_j \zeta_{j-1}}}{\zeta_j + \zeta_{j-1}} \tag{A3a}$$

$$\sigma_{j-1/2} = \frac{\zeta_j - \zeta_{j-1}}{\zeta_j + \zeta_{j-1}}. \tag{A3b}$$

Since $\tau^2_{j-1/2} + \sigma^2_{j-1/2} = 1$, the reflection-transmission matrices are orthogonal and we get the energy conservation law for the Goupillaud medium in the form

$$\sum_{j\in\mathbb{Z}} \big(D_j^2(t) + U_j^2(t)\big) = \sum_{j\in\mathbb{Z}} \big(D_j^2(t+\Delta t) + U_j^2(t+\Delta t)\big). \tag{A4}$$

These equations allow us to characterize the solution at any point in space and time. More precisely, we get the solution at the midpoint of the layers using steps in time equal to the travel time between interfaces. Note that all the analysis above can be made by setting Δx equal to an integer fraction of the travel time across the layers.

[1] M. Fink, Sci. Am. **November**, 91 (1999).
[2] M. Fink, J. Phys. D: Appl. Phys. **26**, 1333 (1993).
[3] P. Blomgren, G. Papanicolaou, and H. Zhao, J. Acoust. Soc. Am. **111**, 230 (2002).
[4] G. Bal and L. Ryzhik, C.R. Acad. Sci. Paris **333**, 1041 (2001).
[5] J. Thomas and M. Fink, IEEE Trans. Ultrason. Ferroelectr. Freq. Control **43**, 1122 (1996).
[6] W. Kuperman, W. Hodgkiss, H. Song, T. Akal, C. Ferla, and D. Jackson, J. Acoust. Soc. Am. **103**, 25 (1997).
[7] R. Burridge, G. Papanicolaou, P. Sheng, and B. White, SIAM J. Appl. Math. **49**, 582 (1989).
[8] M. Asch, G. Papanicolaou, M. Postel, P. Sheng, and B. White, Wave Motion **12**, 429 (1990).
[9] R. Burridge, G. Papanicolaou, and B. White, SIAM J. Appl. Math. **47**, 146 (1987).
[10] G. Bal, G. Papanicolaou, and L. Ryzhik, Stochastics and Dynamics **2**, 507 (2002).
[11] A. Derode, P. Roux, and M. Fink, Phys. Rev. Lett. **75**, 4206 (1995).
[12] A. Derode, A. Tourin, and M. Fink, Phys. Rev. E **64**, 6606 (2001).
[13] M. Fink and C. Prada, Wave Motion **20**, 151 (1994).
[14] J. Clouet and J.-P. Fouque, Wave Motion **25**, 361 (1997).
[15] P. Anderson, Phys. Rev. **109**, 1491 (1958).
[16] A. Kim, P. Blomgren, and G. Papanicolaou, submitted (2003).
[17] D. Alfaro Vigo, J.-P. Fouque, J. Garnier, and A. Nachbin, Stoch. Processes Appl. **113**, 289 (2004).
[18] J.-P. Fouque, J. Garnier, J. Muñoz, and A. Nachbin, Phys. Rev. Lett. **92**, 094502 (2004).
[19] J. Garnier and A. Nachbin, Phys. Rev. Lett. **accepted** (2004).
[20] K. Sølna, Waves Random Media **12**, 365 (2002).
[21] M. Haider, K. Mehta, and J.-P. Fouque, Waves in Random Media **14**, 185 (2004).
[22] J.-P. Fouque, in *Diffuse Waves in Complex Media*, edited by J.-P. Fouque (Kluwer Academic Publishers, The Netherlands, 1999), pp. 319–345.
[23] M. Asch, W. Kohler, G. Papanicolaou, M. Postel, and B. White, SIAM Review **33**, 519 (1991).
[24] B. Engquist, in *Nonlinear Hyperbolic Problems*, edited by C. Carasso, P.-A. Raviart, and D. Serre (Springer-Verlag, New York, 1987), vol. 1270 of *Lectures Notes in Mathematics*, pp. 10–22.
[25] B. Engquist and T. Hou, SIAM J. Numer. Anal. **26**, 289 (1989).
[26] G. Strang, SIAM J. Numer. Anal. **5**, 506 (1968).
[27] A. Pazy, *Semigroups of linear operators and applications to partial differential equations*, vol. 44 of *Applied Mathematical Sciences* (Springer-Verlag, New York, 1983).
[28] J.-P. Fouque and A. Nachbin, Multiscale Model. Simul. **1**, 609 (2003).
[29] B. Engquist and T. Hou, *Computation of oscillatory solutions to hyperbolic differential equations using particle Methods* (Springer-Verlag, New York, 1988), vol. 1360 of *Lectures Notes in Mathematics*, pp. 68–82.
[30] R. O'Doherty and N. Anstey, Geophysical Prospecting **19**, 430 (1971).
[31] P. Sheng, Z. Zhang, B. White, and G. Papanicolaou, Phys. Rev. Lett. **57**, 1000 (1986).
[32] B. White, P. Sheng, and Z. Zhang, Phys. Rev. Lett. **59**, 1018 (1987).